Inorganic Chemistry
Article

Inorg. Chem. **2010**, *49*, 3169–3182 **3169**
DOI: 10.1021/ic901949a

Nucleation of Antiferromagnetically Coupled Chromium Dihalides: from Small Clusters to the Solid State

Brian Vest,[†] Andreas Hermann,[†,⊥] Peter D. W. Boyd,[‡] and Peter Schwerdtfeger*[,†]

[†]*Centre for Theoretical Chemistry and Physics* (*CTCP*), *New Zealand Institute for Advanced Study* (*NZIAS*), *Massey University Albany, Private Bag 102904, North Shore MSC, Auckland, New Zealand, and* [‡]*Department of Chemistry, The University of Auckland, Private Bag 92019, Auckland, New Zealand.* [⊥] *Present address: Department of Chemistry, The University of Auckland, Private Bag 92019, Auckland, New Zealand.*

Received October 8, 2009

The nucleation of chromium dihalide clusters is investigated by studying clusters of the form Cr_nX_{2n} ($n \leq 4$, X = F, Cl, Br, and I) for different spin states and the corresponding low temperature solid-state modifications using density functional theory. Using both wave function based (coupled cluster) and density functional theory, we predict that in all cases the ground state of the CrX_2 monomer is a bent $^5B_2$ state arising from a weakly Renner−Teller distorted $^5\Pi_g$ state of the linear CrX_2 unit. These quintet units can form antiferromagnetically coupled, two-dimensional chains with chromium being bridged by two halides and a nucleation growth pattern that resembles the structural motif found for the solid state. Deviations from this two-dimensional chain growth are only found for the trimers and tetramers of $CrBr_2$ and CrI_2, where a "triangular" three-dimensional geometry takes slight precedence over the planar ribbon motif. We find that each single CrX_2 unit adds an almost constant amount of energy between 45 and 50 kcal/mol to the cluster growth. This is in accordance with the calculated sublimation energies for the solid state which gave 58 kcal/mol for CrF_2, and between 41 and 46 kcal/mol for $CrCl_2$, $CrBr_2$, and CrI_2. The large deviation of the calculated from the experimental sublimation energy for CrF_2 is due to the high electronegativity of fluorine ligand, which substantially increases the ionic interactions, resulting in a much more tightly packed solid-state structure, which is not so well described by spin-broken density functional theory. In accordance with this, CrF_2 shows an unusually large bulk modulus (395 kbar) compared to the heavier halides $CrCl_2$ (82 kbar), $CrBr_2$ (40 kbar), and CrI_2 (18 kbar).

Introduction

The accurate simulation of the nucleation process of atoms or molecules in the gas phase toward the liquid or solid state remains one of the fundamental problems in materials science.[1,2] Even for the simplest interacting systems like neon or argon, where one considers the weak interaction between the rare gas atoms as well understood, it was demonstrated only very recently that the stabilization of the face centered cubic (*fcc*) over the hexagonal closed packed (*hcp*) phase is due to quantum fluctuations.[3] However, for these simple rare gas systems it is still not known at what cluster size or range the nucleation starts to change its growth pattern from the observed icosahedral cluster arrangement to the *fcc* phase observed in the solid state.[4,5] Different cluster polymorphs are often separated by small energies and activation barriers, requiring an accurate quantum theoretical treatment and taking dynamic aspects into account to consider finite temperature effects.[1,5] For metallic clusters the situation is far more complicated, as the transition to the metallic phase in finite clusters is often not accurately known. A prime example here is the simulation of mercury clusters and its solid state.[6]

One might assume that the nucleation of ionic systems such as NaCl, or ionic molecules of the more general form $M^+(X_n)^-$, is much better understood, as the interaction between the charged atoms or molecular dipoles will simply maximize

*To whom correspondence should be addressed. E-mail: peter.schwerdtfeger@gmail.com.

(1) Kashiev, D. *Nucleation*; Butterworth-Heinemann: Oxford, 2000.
(2) Schmelzer, J. W. P *Nucleation Theory and Applications*; Wiley-VCH: Weinheim, 2005.
(3) (a) Rosciszewski, K.; Paulus, B.; Fulde, P.; Stoll, H. *Phys. Rev. B* **1999**, *60*, 7905. (b) Rosciszewski, K.; Paulus, B.; Fulde, P.; Stoll, H. *Phys. Rev. B* **2000**, *62*, 5482. (c) Schwerdtfeger, P.; Gaston, N.; Krawczyk, R. P.; Tonner, R.; Moyano, G. E. *Phys. Rev. B* **2006**, *73*, 064112. (d) Moyano, G. E.; Schwerdtfeger, P.; Rosciszewski, K. *Phys. Rev. B* **2007**, *75*, 024101.
(4) (a) Wales, D. J.; Doye, J. P. K. *J. Phys. Chem. A* **1997**, *101*, 5111. (b) van de Waal, B. W. *Phys. Rev. Lett.* **1996**, *76*, 1083.
(5) Doye, J. P. K.; Calvo, F. *Phys. Rev. Lett.* **2001**, *86*, 3570.
(6) (a) Paulus, B.; Rosciszewski, K.; Stoll, H.; Gaston, N.; Schwerdtfeger, P. *Phys. Rev. B* **2004**, *70*, 165106. (b) Schwerdtfeger, P.; Wesendrup, R.; Moyano, G. E.; Sadlej, A. J.; Greif, J.; Hensel, F. *J. Chem. Phys.* **2001**, *115*, 7401. *J. Chem. Phys.* Corrigendum **2002**, *117*, 6881. (c) Moyano, G. E.; Wesendrup, R.; Söhnel, T.; Schwerdtfeger, P. *Phys. Rev. Lett.* **2002**, *89*, 103401. (d) Gaston, N.; Schwerdtfeger, P. *Phys. Rev. B* **2006**, *74*, 024105. (e) Gaston, N.; Paulus, B.; Rosciszewski, K.; Schwerdtfeger, P.; Stoll, H. *Phys. Rev. B* **2006**, *74*, 094102.

Published on Web 03/02/2010

the electrostatic interaction in a cluster or the solid state.[7] However, even here one can find unexpected growth patterns leading to unusual solid-state structures, as for example highlighted recently for the gold halides[8] or for mercury oxide.[9] For ionic transition metal compounds, one faces further complications as close-lying spin-states can lead to different magnetic phases.[10] In that sense, the chromium dihalides represent a very difficult class of molecules to be studied experimentally or theoretically. These molecules have a d^4 configuration on the metal center, and according to simple ligand-field (LFT) arguments,[11] the transition metal dihalides should all be linear ($D_{\infty h}$ symmetry) with the energetic ordering of the metal d-orbitals being $\delta_g < \pi_g < \sigma_g$. Hence, LFT predicts that the ground state of the chromium dihalides should be the $^5\Sigma_g^+$ state with a $\delta_g^2\pi_g^2$ electron configuration on Cr. Two of the earliest ab initio studies of $CrCl_2$ were in agreement with this prediction.[12] Later, density functional (DFT) calculations[13] showed that the d-electron configuration of the metals is highly dependent on the inclusion of electron correlation, and they predicted that the relative ordering of linear $CrCl_2$ should be $^5\Pi_g$ ($\delta_g^2\pi_g^1\sigma_g^1$) < $^5\Sigma_g^+$ ($\delta_g^2\pi_g^2$) < $^5\Delta_g$ ($\delta_g^1\pi_g^2\sigma_g^1$) instead of $^5\Sigma_g^+ < {}^5\Pi_g < {}^5\Delta_g$ as predicted by LFT. Bridgeman also suggested that some of the early transition metal dihalides could have bent minima with shallow bending potentials.[13] Jensen[14] reported a $^5B_2$ ground state for $CrCl_2$ as a result of Renner−Teller type distortion of the $^5\Pi_g$ state for the first time, followed by Nielsen et al.[15] who predicted the same ground state for CrF_2 and $CrCl_2$ from coupled cluster and DFT calculations. Bending the linear CrX_2 molecule toward C_{2v} symmetry results in further stabilization of the σ_g orbital, with the π_g orbital in the bending plane as well as the δ_g orbitals becoming higher in energy. We note that previous electron diffraction (ED) experiments on CrF_2[16] and $CrCl_2$[17,18] as well as the infrared (IR) spectroscopic studies of all of the chromium dihalides[19−22] all predicted that these molecules are linear in the gas phase. From the IR studies, the lack of an IR-active symmetric stretching mode was indicative of a linear geometry. This stretching mode, however, would be difficult to detect for quasi-linear molecules with very shallow bending potentials as its signal would be weak. Moreover, mass spectrometric studies of $CrCl_2$[23,24] and $CrBr_2$[23] and the gas phase IR study of CrI_2[22] have indicated that the vapor-phase is complex, with oligomers up to the tetramers being present. Oligomer contamination was responsible for the initial misinterpretation of the ED data for $CrCl_2$,[17] and we recently resolved the structure of $CrCl_2$ by a combined use of ED and high-level computations,[25] with the new ED data in agreement with a bent structure for $CrCl_2$. Our calculations showed that the oligomers of $CrCl_2$ consisted of planar ribbons of dichloride-bridged, antiferromagnetically coupled monomers with structural and magnetic properties quite similar to those of their crystals.[26−29] The agreement between theory and experiment for $CrCl_2$ prompted us recently to perform a reanalysis of the original ED experiment of CrF_2 by Zasorin et al.[16] Our results showed that the combination of the high temperature of the ED experiment with many low-lying energy states meant that the CrF_2 molecule should be represented as a weighted mean of low-lying states, rather than just a single state (dynamic analysis).[30]

Moving down the periodic table to the dibromides and diiodides of chromium, we might predict the Renner−Teller distortion to be suppressed as the softer, heavier halides lead to less polarization of the 3d valence shell on Cr, and one might end up with a linear or quasi-linear geometry.[18] Moreover, the larger halides will tend to undergo stronger steric repulsion which favors a linear geometry as well. We also expect competing effects in the determination of the ground electronic states for the larger halides. First, the Cr−Br and Cr−I distances are much larger than those of F or Cl. According to the simple crystal-field approach, this effect will tend to make the 3d energy levels on Cr more closely spaced, leading to possible quasi-degenerate electronic states. Br and I are also much worse σ donors and better π donors than F and Cl, which will tend to raise the energy of the π_g orbitals and lower the energy of the σ_g orbital.

There have only been a few experimental and theoretical investigations on $CrBr_2$ and CrI_2. In the IR analysis of $CrBr_2$,[20] Kovba mentioned that significant amounts of the dimer was present. To make the situation worse, the source of $CrBr_2$ came from the decomposition of $CrBr_3$, with the vapor containing large amounts of $CrBr_3$, $CrBr_4$, and Br_2, making the interpretation of the dimer vibrations very difficult. In the gas-phase IR analysis of CrI_2 by Konings et al.,[22] again, the source of the chromium dihalide came from the decomposition of the trihalide. Konings reported that it was difficult to

(7) Wakisaka, A. *Faraday Discuss.* **2007**, *136*, 299.
(8) (a) Söhnel, T.; Hermann, H. L.; Schwerdtfeger, P. *Angew. Chem., Int. Ed.* **2001**, *40*, 4381. (b) Söhnel, T.; Hermann, H. L.; Schwerdtfeger, P. *J. Phys. Chem. B* **2005**, *109*, 526. (c) Krawczyk, R. P.; Hammerl, A.; Schwerdtfeger, P. *Chem. Phys. Chem.* **2006**, *7*, 2286.
(9) Biering, S.; Hermann, A.; Furthmüller, J.; Schwerdtfeger, P. *J. Phys. Chem. A* **2009**, *113*, 12427.
(10) Hermann, A.; Schwerdtfeger, P. *J. Phys. Chem. A* **2009**, *113*, 12022.
(11) (a) DeKock, C. W.; Gruen, D. M. *J. Chem. Phys.* **1966**, *44*, 4387. (b) DeKock, C. W.; Gruen, D. M. *J. Chem. Phys.* **1968**, *49*, 4521.
(12) (a) Garner, C. D.; Hillier, I. H.; Wood, C. *Inorg. Chem.* **1978**, *17*, 168. (b) Smith, S.; Hillier, I. H. *J. Chem. Soc. Chem. Comm.* **1989**, 539.
(13) (a) Bridgeman, A. J.; Bridgeman, C. H. *Chem. Phys. Lett.* **1997**, *272*, 173. (b) Wang, S. G.; Schwarz, W. H. E. *J. Chem. Phys.* **1998**, *109*, 7252.
(14) Jensen, V. R. *Mol. Phys.* **1997**, *91*, 131.
(15) Nielsen, I. M. B.; Allendorf, M. D. *J. Phys. Chem. A* **2005**, *109*, 928.
(16) Zasorin, E. Z.; Gershikov, A. G.; Spiridonov, V. P.; Ivanov, A. A. *Zh. Strukt. Khim.* **1987**, *28*, 56.
(17) Hargittai, M.; Dorofeeva, O. V.; Tremmel, J. *Inorg. Chem.* **1985**, *24*, 3963.
(18) Hargittai, M. *Chem. Rev.* **2000**, *100*, 2233.
(19) (a) Hastie, J. W.; Hauge, R.; Margrave, J. L. *Chem. Commun.* **1969**, 1452. (b) Hastie, J. W.; Hauge, R.; Margrave, J. L. *High Temp. Sci.* **1971**, *3*, 257. (c) Buchmarina, V. N.; Gerasimov, A. Y.; Predtechenskii, Y. B.; Shklyarik, V. G. *Opt. Spektrosk.* **1988**, *65*, 876. (d) Jacox, M. E.; Milligan, D. E. *J. Chem. Phys.* **1969**, *51*, 4143. (e) Ogden, J. S.; Wyatt, R. S. *J. Chem. Soc. Dalton. Trans.* **1987**, 859. (f) Konings, R. J. M. *High Temp. Mater. Sci.* **1996**, *35*, 105.
(20) Kovba, V. M. *Zh. Neorg. Khim.* **1983**, *28*, 2689.
(21) Gregory, P. D.; Ogden, J. S. *J. Chem. Soc., Dalton Trans.* **1995**, 1423.
(22) Konings, R. J. M.; Booij, A. S. *J. Mol. Struct.* **1992**, *269*, 39.
(23) Schoonmaker, R. C.; Friedman, A. H.; Porter, R. F. *J. Chem. Phys.* **1959**, *31*, 1586.
(24) Ratkovskii, P. A.; Pribitkova, T. A.; Galickii, P. V. *Teplofiz. Vys. Temp.* **1974**, *12*, 731.
(25) Vest, B.; Varga, Z.; Hargittai, M.; Hermann, A.; Schwerdtfeger, P. *Chem.—Eur. J.* **2008**, *14*, 5130.
(26) (a) Hagiwara, M.; Katsumata, K. *J. Magn. Magn. Mater.* **1995**, *140*, 1665. (b) Winkelmann, M.; Baehr, M.; Reehuis, M.; Steiner, M.; Hagiwara, M.; Katsumata, K. *J. Phys. Chem. Solids* **1997**, *58*, 481.
(27) Oswald, H. R. *Helv. Chim. Acta* **1961**, *44*, 1049.
(28) Tracy, J. W.; Gregory, N. W.; Lingafelter, E. C.; Dunitz, J. D.; Mez, H.-C.; Rundle, R. E.; Scheringer, C.; Jnr, H. L. Y.; Wilkinson, M. K. *Acta Crystallogr.* **1961**, *14*, 927.
(29) Hermann, A.; Vest, B.; Schwerdtfeger, P. *Phys. Rev. B* **2006**, *74*, 224402.
(30) Vest, B.; Schwerdtfeger, P.; Kolonits, M.; Hargittai, M. *Chem. Phys. Lett.* **2009**, *468*, 143.

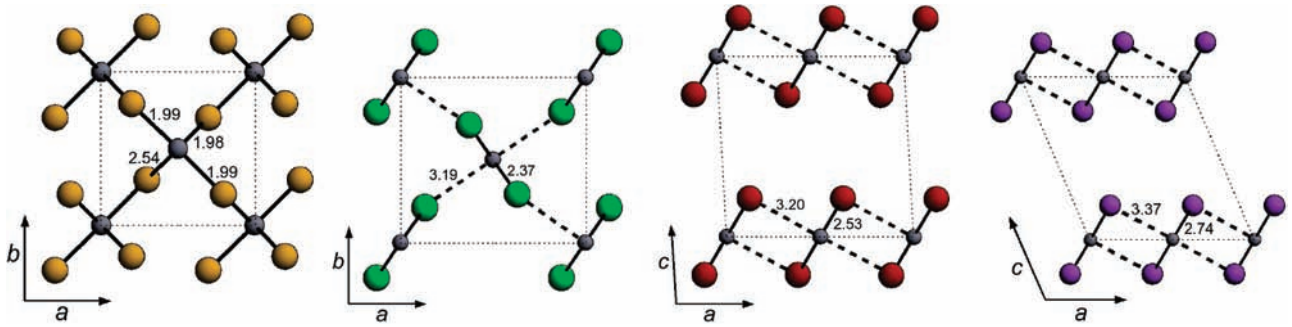

Figure 1. From left to right: optimized crystal structures of antiferromagnetically coupled CrF_2 (space group $P2_1/n$), α-$CrCl_2$ ($Pnnm$), $CrBr_2$ ($C2/m$), and CrI_2 ($C2/m$). Unit cell, crystal axes, and Cr−X bond lengths are indicated.

ascertain whether certain vibrations came from the dimer or from CrI_3 present in the vapor. There has been only one theoretical investigation on CrI_2 and Cr_2I_4. Schiefenhövel et al.[31] calculated a $^5\Pi_g$ ground state for CrI_2 from DFT calculations. Interestingly, this state was a second-order transition state for CrF_2 and $CrCl_2$ from all of our previous calculations, and even our CCSD(T) calculations showed that a bent geometry is lowest in energy.[25,30] Schiefenhövel also mentioned that this state had two real, identical frequencies for bending. They also calculated that the ground state of the CrI_2 dimer consisted of a dihalide-bridged structure of C_{2v} symmetry. Unlike our results for the $CrCl_2$ dimer,[25] Schiefenhövel et al. mentioned that the CrI_2 dimer was not planar, rather the four-membered ring was slightly puckered with a puckering angle of 10.2°.[31] They also calculated a high-spin ($^9B_2$) minimum instead of a low-spin (singlet) state. No other spin states for the dimers were reported, and the trimers and tetramers were not investigated. The solid-state structures of the chromium dihalides all show dihalide-bridged, antiferromagnetically coupled monomer units forming two-dimensional chains which interact such that each chromium is in an (distorted) octahedral environment,[27,28,32] as shown in Figure 1.

Given the complexities of the chromium dihalides and their clusters and the many possible spin-states to be considered on both the theoretical and the experimental fronts, this paper makes a first attempt to discover the trends among the chromium dihalides from fluorine to iodine. Because the structures of the $CrCl_2$ oligomers closely resembled their crystalline structures, we also investigate the geometry and magnetic properties of the oligomers from the dimers to the tetramers as well as the thermodynamics of nucleation for all of the chromium dihalides. Further, we compare the results obtained from our cluster simulations to solid-state calculations to analyze the nucleation growth pattern.

Computational Details

To determine the possible low-energy structures for the $(CrX_2)_n$ (X = F, Cl, Br, and I) clusters, we followed the same procedure as detailed previously for $CrCl_2$[25] by using unrestricted (spin-polarized) Kohn−Sham (UKS) density functional theory, which breaks spin-symmetry in all of these clusters and spin-states (BS-DFT). Preliminary calculations were carried out for a large variety of possible three-dimensional structures with chromium in different coordination and spin states using the PW91 gradient corrected exchange-correlation functional by Perdew et al.[33] together with the Los-Alamos pseudopotentials and corresponding valence double-ζ basis sets (LanL2DZ) for Cr, F, Cl, Br, and I.[34,35] All minima that yielded energies within a window of 0.5 eV from the global minimum were considered for further refinement, except for the tetramer where we chose a window of 0.3 eV because of the high computational costs involved. We refined these calculations by carrying out geometry optimizations with larger basis sets using the PW91 functional. Here we used a modified energy-consistent scalar relativistic small-core pseudopotential from the Stuttgart group with corresponding valence double-ζ basis set with a [8s8p7d3f2g]/(7s7p5d3f2g) contraction scheme for Cr.[36] The basis sets used for F and Cl were an aug-cc-pVDZ basis set,[37] with the cc-pVTZ basis set being used for the monomers as well.[37] The basis sets for Br and I consisted of corresponding augmented double-ζ valence basis set with a [9s8p8d]/(5s4p3d) valence contraction scheme for Br and a [9s7p7d]/(5s4p3d) valence contraction scheme for I,[38] together with energy-consistent, scalar relativistic small-core Stuttgart pseudopotentials. For the CrX_2 dimers, we also performed spin-unrestricted B3LYP[39] geometry optimizations on both the high-spin (nonet) and the low-spin (singlet) states.

The open-shell low- and intermediate spin states of the CrX_2 clusters (X = F, Cl, Br, and I) are all symmetry broken (BS) in a single determinant description and therefore suffer from large spin-contamination. If closed-shell restricted Hartree−Fock (RHF) or Kohn−Sham theory is applied, the corresponding configuration does not even closely resemble the correct singlet ground state. Not surprisingly, we found that the RHF singlet states of dimeric Cr_2X_4 can be more than 10 eV higher in energy than their broken-symmetry unrestricted Hartree−Fock (UHF) structures, the latter showing rather large spin-contamination ($\langle S^2\rangle$ = 4.03 for Cr_2F_4). As one expects, the high-spin nonet state for Cr_2F_4 is an almost pure spin-state in the UKS picture with $\langle S^2\rangle$ = 20.02. We also found significant spin-contaminations for the intermediate

(31) Schiefenhövel, N.; Binnewies, M.; Janetzko, F.; Jug, K. *Z. Anorg. Allg. Chem.* **2001**, *627*, 1513.
(32) (a) Jack, K. H.; Maitland, R. *Proc. Chem. Soc.* **1957**, 232. (b) Tracy, J. W.; Gregory, N. W.; Lingafelter, E. C. *Acta Crystallogr.* **1962**, *15*, 672. (c) Tracy, J. W.; Gregory, N. W.; Stewart, J. M.; Lingafelter, E. C. *Acta Crystallogr.* **1962**, *15*, 460.
(33) Perdew, J. P.; Chevary, J. A.; Vosko, S. H.; Jackson, K. A.; Pederson, M. R.; Singh, D. J.; Fiolhais, C. *Phys. Rev. B* **1992**, *46*, 6671.
(34) Dunning, T. H., Jr.; Hay, P. J. *Methods of Electronic Structure Theory*, Vol. *2*; Schaefer, H. F.; III, Ed.; Plenum Press: New York, 1977.
(35) (a) Hay, P. J.; Wadt, W. R. *J. Chem. Phys.* **1985**, *82*, 270. (b) Hay, P. J.; Wadt, W. R. *J. Chem. Phys.* **1985**, *82*, 299.
(36) Dolg, M.; Wedig, U.; Stoll, H.; Preuss, H. *J. Chem. Phys.* **1987**, *86*, 866.
(37) Dunning, T. H., Jr. *J. Chem. Phys.* **1989**, *90*, 1007.
(38) Peterson, K. A.; Figgen, D.; Goll, E.; Stoll, H.; Dolg, M. *J. Chem. Phys.* **2003**, *119*, 11113.
(39) (a) Vosko, S. H.; Wilk, L.; Nusair, M. *Can. J. Phys.* **1980**, *58*, 1200. (b) Lee, C.; Yang, W.; Parr, R. G. *Phys. Rev. B* **1988**, *37*, 785. (c) Becke, A. D. *J. Chem. Phys.* **1993**, *98*, 5648. (d) Stephens, P. J.; Devlin, F. J.; Chabalowski, C. F.; Frisch, M. J. *J. Phys. Chem.* **1994**, *98*, 11623.

spin-states, and the corresponding total electronic energies deviated significantly from the expected spin-exchange pattern described by a Heisenberg−Dirac−van Vleck Hamiltonian $H = -2J\vec{S}_A\vec{S}_B$ for the two interacting sites A and B producing a spin-ladder of states ranging from $S_A + S_B$ to $|S_A - S_B|$. If we describe the spin-contamination by the parameter m, $\langle S^2_{BS}\rangle = \langle S^2\rangle + m$ (BS = broken symmetry single determinant), we obtain approximately $m = 4$ for the singlet, $m = 3$ for the triplet, $m = 2$ for the quintet, $m = 1$ for the septet, and $m = 0$ for the nonet. Hence, a single-reference description is obviously not sufficient to correctly describe all low- and intermediate spin-states for the oligomers. The correct energy sequence of all weakly coupled spin-states arising from the quintet state of the monomer requires an elaborate multireference treatment (see for example the recent work by Buchachenko et al.[41]) This situation is well-known and has been described intensively in the literature, for example, see the more recent work by Geskin et al.,[42] Kurokawa et al.,[43] or Tabookht et al.[44] Nevertheless, for the dimer the high-spin described by $(S_{Cr1}, S_{Cr2}) = (2, 2)$ and the (spin-contaminated) low-spin solution $(-2, 2)$ came out closest in energy, which we refer to as ferromagnetically coupled (FM) and antiferromagnetically (AFM) coupled states for the following. Moreover, the energy difference between these two states is of the right order of the known intrachain spin-coupling constant in solid $CrCl_2$.[29] Further, to check the accuracy of our AFM and FM UKS calculations, we performed complete active space self-consistent field calculations, CASSCF, followed by second-order perturbation theory, CASPT2,[45,46] for both the monomeric and dimeric species, as well as coupled cluster calculations (CCSD(T)) for the monomer within a full active valence space. For the CASSCF calculations, initial guesses of the wave functions were obtained from restricted open-shell Hartree−Fock calculations. For the low lying $^5\Pi_g$ (and the Renner−Teller distorted $^5B_2$), $^5\Sigma_g^+$ and $^5\Delta_g$ states of the monomers, we applied a CASSCF-(16,15), that is, we distributed 16 electrons in 15 orbitals. This active space consisted of the five 3d metal orbitals on Cr ($\delta_g, \pi_g, \sigma_g$) along with the valence p orbitals from both halides. Also included within the active space were the virtual 4s and 4p orbitals on Cr. The geometry was kept at the optimized DFT structures, as a complete optimization was computationally not feasible. For the CASPT2 calculations, we had to reduce the active space even further to (4,5), which distributes 4 electrons within the metal 3d orbitals. Any attempts to partially include the valence p orbitals on the halides led to root-flipping problems during the perturbation step. We also used the default number of electrons which were correlated in the CASPT2 calculations; the number of correlated electrons for CrF_2, $CrCl_2$, $CrBr_2$, and CrI_2 were 20, 34, 20, and 20, respectively. Here we were able to carry out a geometry optimization for the monomers. For the $^5\Pi_g$ and $^5\Delta_g$ states of the monomer, a state-averaged CASSCF calculation had to be performed to correctly describe the multireference character in these states. For the dimers, we used the same active space as for the monomers, which results in a CASPT2(8,10) of the ten 3d metal orbitals on the Cr atoms. Only the singlet and nonet states of the dimer were examined, as these calculations became again prohibitively computer time expensive, and the geometry was also fixed to that obtained from our DFT calculations. For the monomer, we also carried out DFT calculations using different density functionals for comparison.[39] All unrestricted DFT, CCSD(T), and MP2 calculations were performed using the Gaussian03 software package,[47] and all multireference (CASSCF and CASPT2) calculations were performed using Molpro.[45]

Harmonic vibrational frequencies were computed by standard analytical gradient techniques if available, which gave the zero-point vibrational energy correction, the enthalpy, and the Gibbs free energies of atomization at standard conditions (298.15 K temperature and 1 atm pressure). The binding energies B of the clusters are calculated from the single-point energies of each species in conjunction with the following equations:

$$B_D = E_D - 2E_M \qquad (2CrX_2 \rightarrow Cr_2X_4) \tag{1}$$

$$B_T = E_T - E_D - E_M \qquad (Cr_2X_4 + CrX_2 \rightarrow Cr_3X_6) \tag{2}$$

$$B_Q = E_Q - E_T - E_M \qquad (Cr_3X_6 + CrX_2 \rightarrow Cr_4X_8) \tag{3}$$

$$B_Q' = E_Q - 2E_D \qquad (2Cr_2X_4 \rightarrow Cr_4X_8) \tag{4}$$

where E_M, E_D, E_T, E_Q are the energies of the monomer, dimer, trimer, and tetramer, respectively. Basis set superposition errors (BSSE) for these binding energies were calculated using the counterpoise correction by Boys and Bernardi[48,49] including two-body terms only, and are listed in the Supporting Information (Table **S1**). We note that the BSSE distinguished between the two values B_Q and B'_Q. For all of the clusters, the relative amount of the BSSE is quite small, usually less than 6% of their binding energies, and within the error of the DFT approximation applied. However, although the contribution of the BSSE to the binding energies is small, the actual magnitude of the BSSE is comparable to the energy differences between some of the low-energy oligomers, and in several cases, the errors exceed these

(40) Saito, T.; Kataoka, Y.; Nakanishi, Y.; Matsui, T.; Kitagawa, Y.; Kawakami, T.; Okumura, M.; Yamaguchi, K. *Chem. Phys.* **2010**, *368*, 1.
(41) Buchachenko, A. A.; Chałasiński, G.; Szcześniak, M. M. *J. Chem. Phys.* **2009**, *131*, 241102.
(42) Geskin, V.; Stadler, R.; Cornil, J. *Phys. Rev. B* **2009**, *80*, 085411.
(43) Kurokawa, Y. I.; Nakao, Y.; Sakaki, S. *J. Phys. Chem. A* **2010**, *114*, 1191.
(44) Tabookht, Z.; López, X.; de Graaf, C. *J. Phys. Chem. A* **2010**, *114*, 2028.
(45) Werner, H.-J.; Knowles, P. J.; Lindh, R.; Manby, F. R.; Schütz, M.; Celani, P.; Korona, T.; Rauhut, G.; Amos, R. D.; Bernhardsson, A.; Berning, A.; Cooper, D. L.; Deegan, M. J. O.; Dobbyn, A. J.; Eckert, F.; Hampel, C.; Hetzer, G.; Lloyd, A. W.; McNicholas, S. J.; Meyer, W.; Mura, M. E.; Nicklass, A.; Palmieri, P.; Pitzer, R.; Schumann, U.; Stoll, H.; Stone, A. J.; Tarroni, R.; Thorsteinsson, T. *Molpro, version 2006.1, a package of ab initio programs*; 2006; see http://www.molpro.net.
(46) (a) Wolinski, K.; Pulay, P. *J. Chem. Phys.* **1989**, *90*, 3647. (b) Andersson, K.; Malmqvist, P. A.; Roos, B. O.; Sadlej, A. J.; Wolinski, K. *J. Phys. Chem.* **1990**, *94*, 5483. (c) Celani, P.; Werner, H.-J. *J. Chem. Phys.* **2000**, *112*, 5546. (d) Azizi, Z.; Roos, B. O.; Veryazov, V. *Phys. Chem. Chem. Phys.* **2006**, *8*, 2727.
(47) Frisch, M. J.; Trucks, G. W.; Schlegel, H. B.; Scuseria, G. E.; Robb, M. A.; Cheeseman, J. R.; Montgomery, J. A., Jr.; Vreven, T.; Kudin, K. N.; Burant, J. C.; Millam, J. M.; Iyengar, S. S.; Tomasi, J.; Barone, V.; Mennucci, B.; Cossi, M.; Scalmani, G.; Rega, N.; Petersson, G. A.; Nakatsuji, H.; Hada, M.; Ehara, M.; Toyota, K.; Fukuda, R.; Hasegawa, J.; Ishida, M.; Nakajima, T.; Honda, Y.; Kitao, O.; Nakai, H.; Klene, M.; Li, X.; Knox, J. E.; Hratchian, H. P.; Cross, J. B.; Bakken, V.; Adamo, C.; Jaramillo, J.; Gomperts, R.; Stratmann, R. E.; Yazyev, O.; Austin, A. J.; Cammi, R.; Pomelli, C.; Ochterski, J. W.; Ayala, P. Y.; Morokuma, K.; Voth, G. A.; Salvador, P.; Dannenberg, J. J.; Zakrzewski, V. G.; Dapprich, S.; Daniels, A. D.; Strain, M. C.; Farkas, O.; Malick, D. K.; Rabuck, A. D.; Raghavachari, K.; Foresman, J. B.; Ortiz, J. V.; Cui, Q.; Baboul, A. G.; Clifford, S.; Cioslowski, J.; Stefanov, B. B.; Liu, G.; Liashenko, A.; Piskorz, P.; Komaromi, I.; Martin, R. L.; Fox, D. J.; Keith, T.; Al-Laham, M. A.; Peng, C. Y.; Nanayakkara, A.; Challacombe, M.; Gill, P. M. W.; Johnson, B.; Chen, W.; Wong, M. W.; Gonzalez, C.; Pople, J. A. *Gaussian 03*, Revision C.03; Gaussian, Inc.: Wallingford, CT, 2004.
(48) Boys, S. F.; Bernardi, F. *Mol. Phys.* **1970**, *19*, 533.
(49) van Duijneveldt, F. B.; van Duijneveldt-van de Rijdt, J. G. C. M.; van Lenthe, J. H. *Chem. Rev.* **1994**, *94*, 1873.

energy differences. Nevertheless, they remain fairly constant within different spin states and therefore do not alter the sequence of states. There is only one exception where the nonet state of Cr_2I_4 is no longer lowest in energy. However, the energy difference between the singlet and nonet states of Cr_2I_4 from the DFT calculations is just too small to ascertain which state is lowest in energy.

To calculate the ground state properties of the low-temperature modifications of crystalline CrF_2, α-$CrCl_2$, $CrBr_2$, and CrI_2 we employed DFT in conjunction with a plane wave basis set as implemented in the Vienna Ab-initio Simulation Package.[50] The electron−electron interaction is modeled using the generalized gradient approximation (GGA) by Perdew et al.[33] (PW91) of the exchange-correlation energy. The electron-ion interaction is modeled using the projector augmented wave (PAW) method,[51] restricting the expansion of the Bloch functions to a cutoff of 450 eV. Brillouin zone (BZ) integrations are carried out on a regular mesh in reciprocal space, equivalent to 128 *k*-points in the BZ of the primitive CrX_2 unit cells. To find the minimal energy structure, we optimize the cell lattice vectors and all internal coordinates for a number of given cell volumes, using a conjugate-gradient or quasi-Newton algorithm to minimize the Hellmann−Feynman forces. We consider a structure to be in equilibrium if each Cartesian component of the atomic forces is below 5 meV/Å. We fit the resulting $E(V)$ curve with a Vinet equation of state (EOS),[52] and finally optimize the cell parameters and internal structure at the equilibrium cell volume V_0.

Results and Discussion

Chromium Dihalide Monomers. To discuss all possible low-lying electronic states for the oligomers, we need to discuss briefly the spin-coupling in the CrX_2 monomers, cf. Table 1 (a more complete list of all calculations including the higher lying $^5\Delta_g$, $^3\Sigma_g^-$, and $^1\Sigma_g^+$ states for $CrBr_2$ and CrI_2 can be found in the Supporting Information Tables **S2** and **S3**). A complete listing of all calculations for CrF_2 and $CrCl_2$ have been reported previously[25,30] and will not be repeated here. Both DFT and CCSD(T) predict that the $^5\Pi_g$ state is lowest in energy for the linear structures followed by the $^5\Sigma_g^+$ state. However, the $^5\Pi_g$ state undergoes a Renner−Teller distortion into the bent structure, splitting into two nondegenerate states of $^5B_2$ and $^5A_2$ symmetry, of which the $^5B_2$ state is the ground state as discussed before for CrF_2 and $CrCl_2$.[25,30] Figure 2 summarizes the bending potential curves for the $^5\Pi_g \rightarrow {}^5B_2/{}^5A_2$, and $^5\Sigma_g^+ \rightarrow {}^5A_1$ states of all of the chromium dihalides from our PW91 calculations. We mention that although the PW91 barriers to linearity for CrF_2 and $CrCl_2$ are somewhat higher than the B3LYP values given in refs 25,30, we are primarily concerned in their overall trend going down the halide group. The CASPT2 calculations predict that the $^5\Sigma_g^+$ state is lowest in energy for CrF_2 to $CrBr_2$. However, a limited CAS space was used in these calculations, and given that all of the CCSD(T) calculations predict a $^5B_2$ ground state, we are certain that this state falls below the $^5\Sigma_g^+$ state for all halides. The next state, $^5\Delta_g$, is considerably higher in energy by all methods applied and cannot be considered as a contestant for the ground state. Also, the lower spin triplet and singlet states of the monomers were both significantly higher in energy than the global minima. At elevated temperatures, however, significant mixing among the low lying quintet states $^5B_2(^5\Pi_g)$, $^5A_2(^5\Pi_g)$, and $^5A_1(^5\Sigma_g^+)$ will more than likely occur with the argument of bent versus linear structure breaking down, and it is expected that the chromium dihalides will be quasilinear at this point.[25,30] Nevertheless, the results obtained for the monomers clearly show that it is sufficient to consider the quintet states at one chromium center only to describe all subsequent spin states arising in the cluster formation.

The minimum of the $^5B_2$ state is located at bond angles between 140° for CrF_2 to about 170° for CrI_2, with the bending curves becoming more shallow going down the halide group in the periodic table. Furthermore, the bond angles increase with increasing size of the halide ligand, with a rather large increase by about 25° between $CrBr_2$ and CrI_2 at the PW91 level of theory. A similar trend was also observed for halide complexes of some of the main group elements.[53] For $CrBr_2$, both CASPT2 and

Table 1. Relative Energies (eV), Cr−X Distances (Å), and X−Cr−X Angles (deg) of CrX_2 (X = F, Cl, Br and I) for Different Electronic States[a]

	state	method	ΔE	R(CrX)	∠(XCrX)
CrF_2		exp.[b]		1.785(6)	
	$^5B_2$	PW91	0	1.767	132.8
		CASPT2	0.079	1.795	143.1
		CCSD(T)	0	1.791	149.3
	$^5\Pi_g$	PW91	0.117	1.783	180
		CASPT2	0.161	1.803	180
		CCSD(T)	0.018	1.795	180
	$^5\Sigma_g^+$	PW91	0.493	1.834	180
		CASPT2	0	1.803	180
		CCSD(T)	0.080	1.795	180
$CrCl_2$		exp.[c]		2.196(20)	149(9.5)
	$^5B_2$	PW91	0	2.172	141.5
		CASPT2	0.035	2.201	167.5
		CCSD(T)	0	2.194	167.0
	$^5\Pi_g$	PW91	0.029	2.182	180
		CASPT2	0.085	2.202	180
		CCSD(T)	0.032	2.194	180
	$^5\Sigma_g^+$	PW91	0.402	2.224	180
		CASPT2	0	2.240	180
		CCSD(T)	0.145	2.240	180
$CrBr_2$	$^5B_2$	PW91	0	2.322	148.0
		CASPT2	0.003	2.346	179.9
		CCSD(T)	0	2.329	179.8
	$^5\Pi_g$	PW91	0.009	2.330	180
		CASPT2	0.055	2.347	180
		CCSD(T)	1.4×10^{-4}	2.329	180
	$^5\Sigma_g^+$	PW91	0.452	2.370	180
		CASPT2	0	2.384	180
		CCSD(T)	0.162	2.377	180
CrI_2	$^5B_2$	PW91	0	2.540	174.5
		CASPT2	0	2.554	169.9
		CCSD(T)	0	2.530	167.8
	$^5\Pi_g$	PW91	3.8×10^{-4}	2.540	180
		CASPT2	0.056	2.556	180
		CCSD(T)	0.001	2.531	180
	$^5\Sigma_g^+$	PW91	0.497	2.577	150.8
		CASPT2	0.021	2.591	180
		CCSD(T)	0.208	2.581	180

[a] For all other DFT and wave function based calculations including vibrational frequencies see Supporting Information. [b] Experimental value from ref 30. [c] Experimental value from ref 25.

(50) Kresse, G.; Furthmüller, J. *Phys. Rev. B* **1996**, *54*, 11169.
(51) (a) Blöchl, P. E. *Phys. Rev. B* **1994**, *50*, 17953. (b) Kresse, G.; Joubert, D. *Phys. Rev. B* **1999**, 1758.
(52) Vinet, P.; Ferrante, J.; Smith, J. R.; Rose, J. H. *J. Phys. C: Solid State Phys.* **1986**, *19*, L467.
(53) (a) Atanasov, M.; Reinen, D. *J. Am. Chem. Soc.* **2002**, *124*, 6693. (b) Atanasov, M.; Reinen, D. *Inorg. Chem.* **2004**, *43*, 1998. (c) Atanasov, M.; Reinen, D. *Inorg. Chem.* **2005**, *44*, 5092.

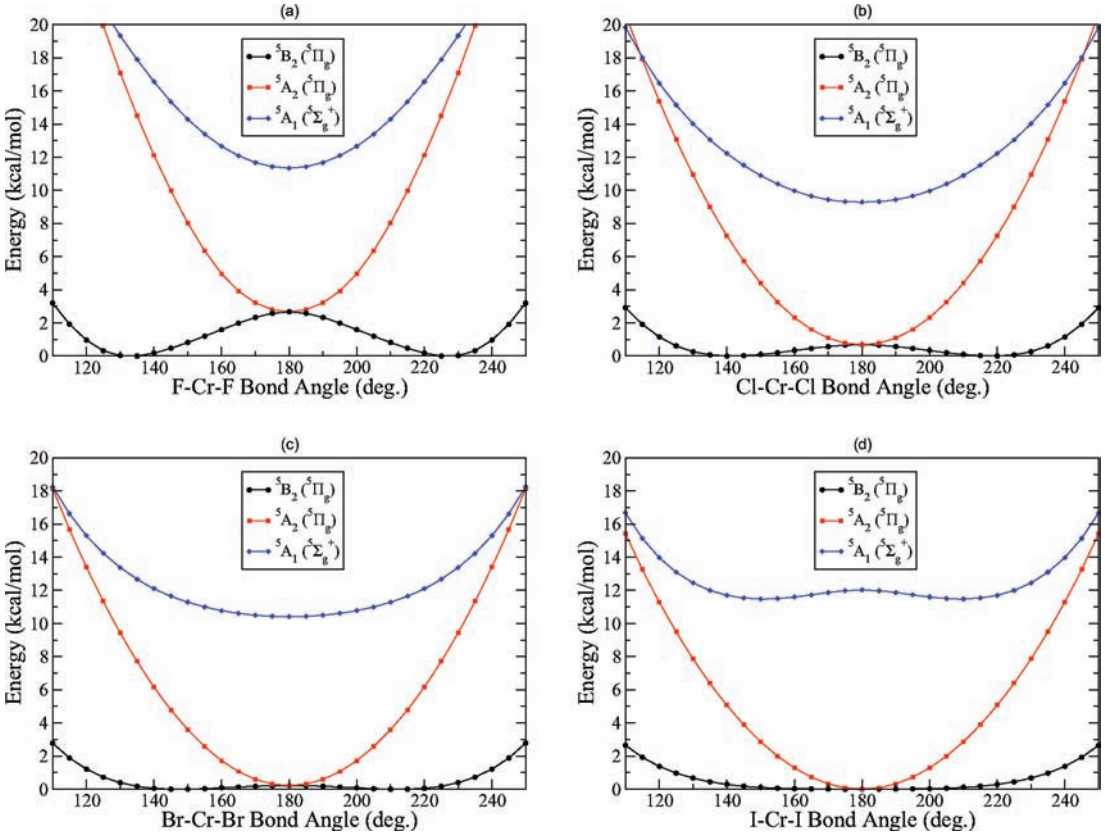

Figure 2. PW91 bending potential curves of the $^5B_2(^5\Pi_g)$, $^5A_2(^5\Pi_g)$, and $^5A_1(^5\Sigma_g^+)$ states for (a) CrF_2, (b) $CrCl_2$, (c) $CrBr_2$, and (d) CrI_2.

CCSD(T) predict bond angles much closer to the linear structure. Nevertheless, the molecules can be considered as quasi-linear, and it is of no surprise that bent structures for transition metal halides have been a matter of dispute for a very long time.[54] What is perhaps surprising is that the $^5A_1/^5\Sigma_g^+$ state becomes a second-order saddle point for CrI_2 at the PW91 level of theory. However, the energy difference from the $^5A_1$ minimum to the linear $^5\Sigma_g^+$ state is only 0.024 eV. Moreover, both CASPT2 and CCSD(T) give linear geometries, that is, we found no other minimum at a bent arrangement.

The results of the Mulliken and NBO analyses for all of the chromium dihalides are given in Table **S4**. As expected, a large portion of the spin is located on the Cr atom with only a small amount present on the halides. The charge on Cr decreases going down the halide group as the electronegativity of the halide ligand decreases, reflecting more covalent and less ionic interactions between the metal atom and the halide. We note that the NBO charges for Cr are significantly more positive than the corresponding Mulliken charges.

Chromium Dihalide Dimers. Combining two bent or linear CrX_2 units, by optimizing the attractive Coulomb interactions between the positively charged chromium atoms and the negatively charged halide ligands, results in either a *cis* or a *trans* doubly bridged Cr_2X_4 cluster depending on the X−Cr−X angle as shown in Figure 3 (dimer structures D1 and D2). Indeed, at the PW91 level of theory the global minimum for Cr_2F_4 to Cr_2Br_4 is an AFM state of either structure (D1) or (D2), whereas the global minimum for Cr_2I_4 is a FM state of D_{2h} symmetry, but this could be an artifact of our UKS treatment. Nevertheless, B3LYP calculations also predicted that the AFM state of (D1) was the global minimum for the CrI_2 dimer and not the FM D_{2h} structure. Their relative energies at different levels of theory are listed in Table 3. Furthermore, the combination of two quintet monomers leads to a sequence of five spin-states, that is, from the singlet to the nonet state. Here we restrict our discussion to the AFM and FM states, which are reasonably well described within our symmetry-broken single-determinant description. The relative energies of some other low-lying FM or AFM dimer minima are given in the Supporting Information (Table **S5**). The AFM and FM states of the dihalide-bridged structures are very close in energy, which agrees with the weak spin coupling and therefore small energy separation between the FM and

Table 2. Lattice Parameters *a*, *b*, *c* (Å) and *β* (deg), Cohesive Energies E_{coh} (eV) per CrX_2 Unit, and Bulk Moduli *B* (kbar) for the Chromium Dihalide Crystals[a]

	CrF_2		$CrCl_2$		$CrBr_2$		CrI_2	
	PW91	exp.	PW91	exp.	PW91	exp.	PW91	exp.
a	4.740	4.73	7.077	6.64	7.399	7.114	7.827	7.545
b	4.696	4.72	6.323	5.98	3.643	3.649	3.938	3.929
c	3.619	3.51	3.451	3.48	7.109	6.217	8.437	7.505
β	98.67	96.50	90.00	90.00	93.60	93.53	113.00	115.31
E_{coh}	2.496		1.978		1.862		1.777	
B	395		82.5		39.9		17.8	

[a] The lattice parameters α and *γ* are 90 degrees. Ferromagnetic coupling between the chromium atoms along the chains were used in our DFT calculations. Experimental values from refs 28,32.

(54) Wilson, A. V.; Roberts, A. J.; Young, N. A. *Angew. Chem., Int. Ed.* **2008**, *47*, 1774.

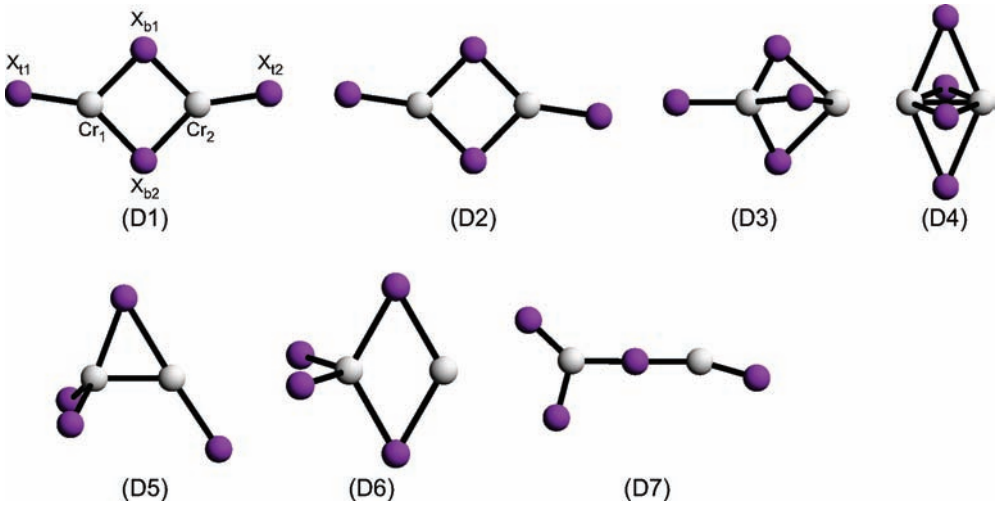

Figure 3. Low energy minima for the chromium dihalide dimers.

Table 3. Relative Energies (eV) among the Lowest Energy Dimers Shown in Figure 3 at the PW91, B3LYP, and CASPT2 Level of Theory

molecule	structure	state[a]	PW91	B3LYP	CASPT2
Cr_2F_4	D1	FM (C_{2v})	0.033	0.015	
		AFM (C_{2v})	0.003	0.001	
	D2	FM (C_{2h})	0.027	0.011	0.006
		AFM (C_{2h})	0	0	0
Cr_2Cl_4	D1	FM (C_{2v})	0.107	0.056	0
		AFM (C_{2v})	0	0	0.024
	D2	FM (C_{2h})	0.121	0.061	
		AFM (C_{2h})	6.1×10^{-5}	4.3×10^{-3}	
Cr_2Br_4	D1	FM (C_{2v})	0.100	0.057	0
		AFM (C_{2v})	0	0	0.018
	D2	FM (C_{2h})	0.102	0.058	
		AFM (C_{2h})	0.001	3.5×10^{-6}	
Cr_2I_4	D1	FM (D_{2h})[b]	0		0
		FM (C_{2v})		0.047	
		AFM (C_{2v})	0.001	0	0.033
	D2	FM (C_{2h})		0.047	
		AFM (C_{2h})	0.004	4.1×10^{-7}	

[a] The symmetry of the molecule is given in parentheses. All dimers are either of A_1 (C_{2v}), A_g (C_{2h}) or A_{1g} (D_{2h}) symmetry. [b] Both the C_{2v} and C_{2h} symmetries for the FM state of Cr_2I_4 (PW91) optimized to a perfect D_{2h} symmetry.

AFM states found in solid $CrCl_2$.[29] The same trends are also seen from our B3LYP calculations; however, for Cr_2I_4, the FM state of the D_{2h} structure represented a second-order saddle point, splitting to structures (D1) and (D2).

Selected geometrical parameters for the lowest energy dimers are given in Table 4. The high symmetry planar D_{2h} structures for both the AFM and FM coupled spin-states of the chromium dihalide dimers represent second-order saddle-points and undergo a pseudo Jahn−Teller distortion toward either the *cis*-(D1) or *trans*-(D2) arrangements, with one exception of the high-spin Cr_2I_4. Figure 4 shows the symmetric in-plane bending potentials ($D_{2h} \rightarrow$ *cis*-(D1)) for the dimer AFM and FM states, with the bending angle of zero degrees representing the D_{2h} structure. The C_{2v} minimum structures for the FM states are well-defined and lie up to 0.5 kcal/mol below the D_{2h} saddle-point (except for Cr_2I_4). In contrast, the bending potentials for the singlet states are very shallow and can be regarded as "pseudo-D_{2h} structures". Unlike the monomer bending potential curves (Figure 2), there seems to be no direct correlation between the size of the halide and potential well toward the high symmetry (D_{2h}) point. This pseudo Jahn−Teller distortion arises from an uneven occupation of eight electrons within ten quasi-degenerate orbitals. The eight highest occupied and two lowest unoccupied orbitals consist primarily of the 3d orbitals of both Cr atoms (nonet state). For the CrF_2 dimer, the ten orbitals are almost entirely metal 3d in character. However, these orbitals mix significantly with the valence p orbitals of the heavier halides. We note that Cr_2I_4 shows the smallest HOMO−LUMO gap (ε_{HL}), that is, going down the group of halides we obtain ε_{HL} = 1.48, 1.08, 0.67, and 0.50 eV for the nonet states of Cr_2F_4, Cr_2Cl_4, Cr_2Br_4, and Cr_2I_4, respectively. This agrees qualitatively with the band gaps obtained from our solid-state calculations (1.07 eV for Cr_2F_4, 1.05 eV for Cr_2Cl_4, 0.84 eV for Cr_2Br_4, and 0.68 eV for Cr_2I_4).

The terminal Cr−X_t distance changes very little between the two different spin states. In fact, most of the differences in bond lengths between the AFM and FM states come from the bridging Cr−X_b and the Cr−Cr distances. As expected, the Cr−Cr distance for the FM states are between 0.03−0.1 Å longer than in the AFM states, and these differences increase from F to Br. The exception to this trend is, again, the FM state of the CrI_2 dimer, whose Cr−Cr distance is significantly shorter compared to the FM state indicating perhaps some Cr−Cr interactions. We note that Schiefenhövel et al.[31] calculated the geometry of the CrI_2 dimer using the local density approximation. They determined that the global minimum of Cr_2I_4 is of C_{2v} symmetry with a $^9B_2$ ground state. In contrast to our result, their optimized structure gave a ring puckering angle of 10.2°. Their calculated bond lengths are significantly shorter than our values, that is, they give Cr−Cr, Cr−I_t, and Cr−I_b distances of 3.000, 2.493, and 2.594 Å, respectively.

In accordance with simple ligand-field theory, the Mulliken spin densities for the dimers show that most of the spin is located on the chromium atoms, with only a small amount being present on the halides, similar to the spin densities found for the monomers (Supporting Information, Table **S6**). The magnitude of spin present on chromium increases with decreasing electronegativity of

Table 4. PW91 Optimized Bond Distances and Angles for the Singlet and Nonet States of Either (D1) or (D2) Minimum Structures[a,b]

molecule	state	parameter	value[c]	molecule	state	parameter	value[c]
Cr_2F_4	FM	$R(Cr_1-Cr_2)$	3.039	Cr_2Br_4	FM	$R(Cr_1-Cr_2)$	3.388
		$R(Cr_1-F_{t1})$	1.791			$R(Cr_1-Br_{t1})$	2.337
		$R(Cr_1-F_{b1})$	1.938			$R(Cr_1-Br_{b1})$	2.447
		$R(Cr_1-F_{b2})$	1.983			$R(Cr_1-Br_{b2})$	2.526
		$\angle(F_{t1}-Cr_1-F_{b1})$	126.3			$\angle(Br_{t1}-Cr_1-Br_{b1})$	116.0
		$\angle(F_{t1}-Cr_1-F_{b2})$	155.3			$\angle(Br_{t1}-Cr_1-Br_{b2})$	149.9
		$\angle(F_{b1}-Cr_1-F_{b2})$	78.4			$\angle(Br_{b1}-Cr_1-Br_{b2})$	94.1
	AFM	$R(Cr_1-Cr_2)$	2.995		AFM	$R(Cr_1-Cr_2)$	3.284
		$R(Cr_1-F_{t1})$	1.791			$R(Cr_1-Br_{t1})$	2.331
		$R(Cr_1-F_{b1})$	1.937			$R(Cr_1-Br_{b1})$	2.467
		$R(Cr_1-F_{b2})$	1.977			$R(Cr_1-Br_{b2})$	2.467
		$\angle(F_{t1}-Cr_1-F_{b1})$	128.2			$\angle(Br_{t1}-Cr_1-Br_{b1})$	131.7
		$\angle(F_{t1}-Cr_1-F_{b2})$	151.6			$\angle(Br_{t1}-Cr_1-Br_{b2})$	131.8
		$\angle(F_{b1}-Cr_1-F_{b2})$	80.2			$\angle(Br_{b1}-Cr_1-Br_{b2})$	96.6
Cr_2Cl_4	FM	$R(Cr_1-Cr_2)$	3.329	Cr_2I_4	FM	$R(Cr_1-Cr_2)$	3.078
		$R(Cr_1-Cl_{t1})$	2.190			$R(Cr_1-I_{t1})$	2.543
		$R(Cr_1-Cl_{b1})$	2.314			$R(Cr_1-I_{b1})$	2.651
		$R(Cr_1-Cl_{b2})$	2.379			$R(Cr_1-I_{b2})$	2.651
		$\angle(Cl_{t1}-Cr_1-Cl_{b1})$	119.5			$\angle(I_{t1}-Cr_1-I_{b1})$	125.5
		$\angle(Cl_{t1}-Cr_1-Cl_{b2})$	150.9			$\angle(I_{t1}-Cr_1-I_{b2})$	125.5
		$\angle(Cl_{b1}-Cr_1-Cl_{b2})$	89.6			$\angle(I_{b1}-Cr_1-I_{b2})$	109.0
	AFM	$R(Cr_1-Cr_2)$	3.181		AFM	$R(Cr_1-Cr_2)$	3.437
		$R(Cr_1-Cl_{t1})$	2.186			$R(Cr_1-I_{t1})$	2.537
		$R(Cr_1-Cl_{b1})$	2.319			$R(Cr_1-I_{b1})$	2.654
		$R(Cr_1-Cl_{b2})$	2.332			$R(Cr_1-I_{b2})$	2.676
		$\angle(Cl_{t1}-Cr_1-Cl_{b1})$	128.1			$\angle(I_{t1}-Cr_1-I_{b1})$	121.5
		$\angle(Cl_{t1}-Cr_1-Cl_{b2})$	138.2			$\angle(I_{t1}-Cr_1-I_{b2})$	138.8
		$\angle(Cl_{b1}-Cr_1-Cl_{b2})$	93.7			$\angle(I_{b1}-Cr_1-I_{b2})$	99.7

[a] For notation of the different structures see Figure 3 and Table ref 3. [b] The global minimum for the nonet state of Cr_2I_4 has D_{2h} symmetry. [c] All bond lengths in Å and all bond angles in degrees.

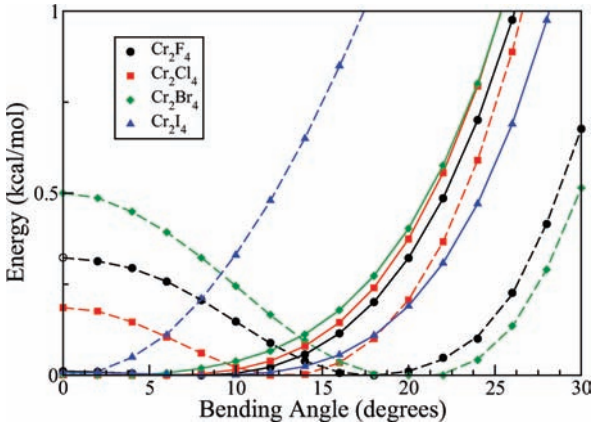

Figure 4. PW91 bending potential curves for the in-plane bending of the terminal halides toward structure (D1) for the AFM (solid lines) and FM (dashed lines) states of the dimers. A bending angle of 0° represents the D_{2h} geometry; all energies are normalized to the respective potential curve minimum.

the halide ligand, as less electron density is withdrawn from the chromium atom. All of the AFM electronic states are of broken spin-symmetry, with one chromium atom having an excess of roughly four α electrons, and the other a concomitant excess of β electrons, which are mainly of 3d-orbital character. The primary disadvantage of BS-DFT is that the exchange coupling between the metal centers is overestimated, and the coupled-spin states are overstabilized.[55] Not only this, but we obtained $\langle S^2\rangle$ values of 4.03, 3.96, 4.00, and 4.08 for the AFM states of Cr_2F_4, Cr_2Cl_4, Cr_2Br_4, and Cr_2I_4, respectively. These results indicate a significant amount of spin-contamination, which we briefly discuss for the dimer in the following.

In an attempt to correct for spin-contamination, we applied the spin-projection method as described in detail by Yamaguchi and co-workers,[56] that is, we have for a specific spin-state S

$$E^{(S)} = E_{BS}^{(S)} + f_{SC}(E_{BS}^{(S)} - E_{BS}^{(FM)}) \quad (5)$$

where BS refers to the broken-symmetry single-determinant solution (for each spin), FM to the high-spin ferromagnetic state, and f_{SC} to the spin-contamination factor, which can easily be determined from the m values given in the computational section. This gives $f_{SC} = 1/4$ for the singlet, $f_{SC} = 3/17$ for the triplet, $f_{SC} = 1/6$ for the quintet, $f_{SC} = 1/7$ for the septet, and $f_{SC} = 0$ for the nonet state. Applying these corrections, we get the spin singlet state as the lowest energy state, followed by the nonet, then triplet, then septet, and finally quintet (at the optimized nonet geometry). Hence, it does not follow the simple Heisenberg picture in the symmetry-broken DFT approach, which comes at no surprise as the system is inherently multiconfigurational. Moreover, in this picture the intermediate spin-states still lie more than 1 eV above the singlet state. At the LanL2DZ/B3LYP level, the energy differences to the low-spin singlet are 1.04 eV for the triplet, 1.41 eV for the quintet, 1.03 eV for the septet, and 0.005 eV for the nonet state of Cr_2F_4, and at the PW91 level using the larger basis sets and Stuttgart pseudopotential we get 0.92 eV for the triplet, 1.25 eV for

(55) Rudra, I. R.; Wu, Q.; Voorhis, T. V. *J. Chem. Phys.* **2006**, *124*, 9.

(56) (a) Yamanaka, S.; Okumura, M.; Nakano, M.; Yamaguchi, K. *J. Mol. Struct. (Theochem)* **1994**, *310*, 205. (b) Nishino, M.; Yamanaka, S.; Yoshioka, Y.; Yamaguchi, K. *J. Phys. Chem. A* **1997**, *101*, 705.

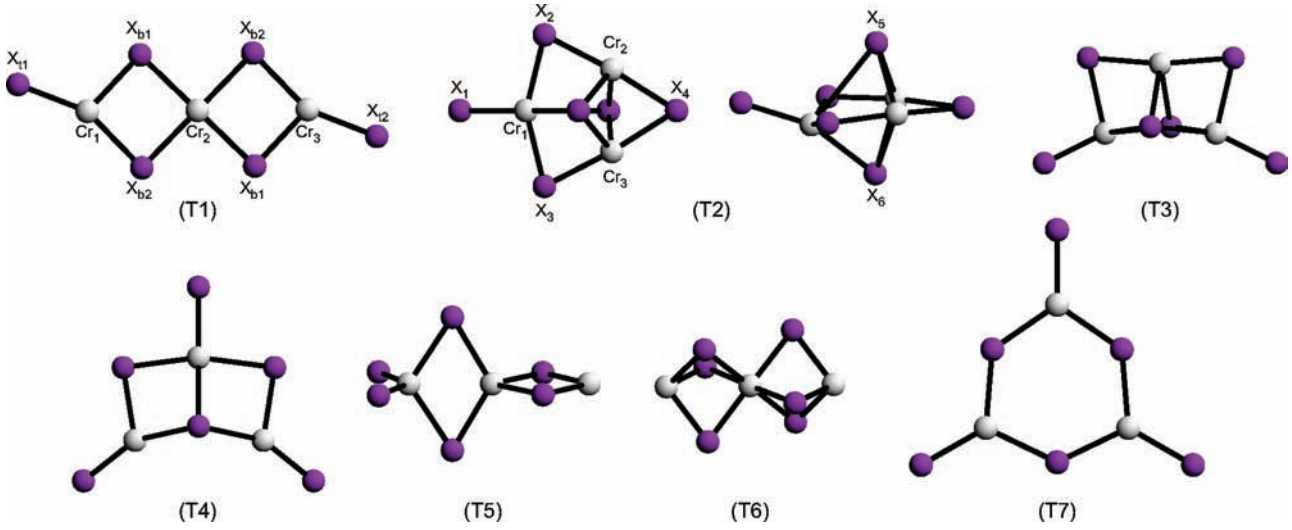

Figure 5. Low energy minima for the chromium dihalide trimers.

the quintet, 0.99 eV for the septet, and 0.02 eV for the nonet state respectively. A look at the spin densities shows that these intermediate spin states mix in the other low-spin states at a single Cr center. Nevertheless, the corrected spin-coupling constants J (obtained from the AFM and FM states using Noodleman's broken-symmetry model[57] which gives $J = -(E_{FM} - E_{AFM})/(S_A + S_B)^2$) are all small (less than 0.01 eV) for the dimers. For example, for Cr_2Cl_4 we get $J = -6.6 \times 10^{-3}$ eV (PW91) and -3.5×10^{-3} eV (B3LYP), and therefore larger in size compared to the intra-chain spin-coupling known experimentally for solid $CrCl_2$ (-8×10^{-4} eV).[26,29] While these spin-coupling constants for the dimer and the solid-state are not strictly comparable, we emphasize again that for correctly describing spin-coupling in transition metal halides, multireference configuration interaction methods are required, and the DFT results can only be taken as estimates (see also a recent discussion by Saito et al.[40]). For example, in a recent paper by Buchachenko on the Europium dimer, the Heisenberg model was nicely followed within a multireference treatment, but it was shown that the spin-coupling constant is very dependent on the model used and even changes sign from a CASSCF to a more accurate MRCI treatment.[41] We note that our single-point CASPT2 values for Cr_2Cl_4 gives $J = 0.0024$ eV; thus, we have a sign change compared to DFT which could be due to the fact that we did not optimize the structures at the CASPT2 level of theory. Nevertheless, to compare to our DFT results for Cr_2F_4 as shown above, we carried out additional CASPT2 calculations at the fixed nonet PW91 geometry. Here the energy differences to the low-spin singlet are 0.0019 eV for the triplet, 0.0052 eV for the quintet, 0.0092 eV for the septet, and 0.0128 eV for the nonet state, which gives a rather small J-value of -6.4×10^{-4} eV, and the intermediate states deviate substantially from the Lande interval rule. (NB: these calculations are carried out with a fixed geometry and without a frozen core, and the energy difference deviates from the one given in Table 3). Here we note that the simple Heisenberg model may not always be applicable.[43]

(57) (a) Noodleman, L. *J. Chem. Phys.* **1981**, *74*, 5737. (b) Noodleman, L.; Davidson, E. R. *Chem. Phys.* **1986**, *109*, 131.

Moreover, structural changes caused by pseudo-Jahn–Teller effects for different spin-states in our chromium dihalides lead to a breakdown of this simple Heisenberg model. Nevertheless, beside this effect, the energy separation and structural differences between the low- and high-spin states in BS-DFT are rather small in accordance with the results found for the magnetic states of solid $CrCl_2$.[29] This gives us some confidence that BS-DFT, indeed, leads to useful energetics and structures in the cluster formation. Moreover, we are primarily concerned with the relative energetic ordering and geometries of the lowest energy structures. A comparison of spin-projected coupling constants, although useful, is not our primary focus in this paper.

To further check the reliability of our BS-DFT approach, we performed CASPT2(8,10) calculations on the lowest energy singlet and nonet states with their structures fixed at those obtained from our DFT geometry optimizations, see Table 3. We mention that restricted open-shell Hartree–Fock calculations predict very high lying singlet states, between 8 and 21 eV above the nonet states, and are therefore useless, clearly demonstrating the multireference character of this state. This singlet state drops substantially in energy in a CASSCF(8,10) treatment, lying less than 0.095 eV above the nonet state for all the dimers, and further decreases in a CASPT2 calculation. Hence, for the correct ordering of the states, dynamic correlation is required. The CASPT2 calculations predict high-spin ground states for Cr_2Cl_4 to Cr_2I_4, but a singlet ground state for Cr_2F_4. Not surprisingly, the singlet states for all of the dimers have significant multireference character, and they all consist of more than 100 major configurations with |CI-coefficients| > 0.05. Hence, for the chromium dihalide dimers we can currently not predict the correct ordering of the spin states, and a much larger dynamic electron correlation space is required together with a geometry optimization to correctly describe the magnetic ordering in these clusters. Consequently, we rely on our BS-DFT calculations in our further cluster studies.

Chromium Dihalide Trimers. The coupling of three quintet CrX_2 units for the trimers (T) results in seven

spin states, where we only consider the AFM and FM states with structures shown in Figure 5. The relative energies among all of the low-lying minima are given in the Supporting Information (Table **S7**), and only the data of the lowest energy trimers are collected in Table 5. For Cr_3F_6 and Cr_3Cl_6, a continuation of the AFM coupled, planar ribbons (T1) is lowest in energy. However, for Cr_3Br_6 and Cr_3I_6 we obtain a three-dimensional AFM state (T2) as the preferred minimum. Obviously, the tendency of three-dimensional cluster growth through structure (T2) becomes more prominent going down the halide group. The (T2) structure consists of three Cr atoms lying within a triangular plane, in contrast to the linear (T1) arrangement. Within this structure are three slightly out-of-plane monohalide bridges (X_2, X_3, X_4, cf. Figure 5) linking the three Cr atoms. Two additional halides (X_5 and X_6) cap the cluster above and below the plane of the Cr atoms, and are bonded to all three of the Cr atoms. Finally, there is a "terminal" halide (X_1) attached to Cr_1. Examining the solid-state structures of $CrBr_2$ and CrI_2 (see Figure 1), we note that we cannot find structure (T2) as a subunit. However, the AFM states for all of the C_{2h} structures (T1) lie less than 0.105 eV higher in energy than their corresponding FM states. It is therefore difficult to predict how important such 3D structures are in the nucleation process. Moreover, for the FM states we obtain much higher energies for the (T2) structures.

Selected geometrical parameters for the trimer global minima are given in the Supporting Information, Table **S8**, with the atomic labeling schemes given in Figure 5.

Table 5. Relative Energies (eV) among the Lowest Energy Trimers Shown in Figure 5 at the PW91/LanL2DZ and PW91/aug-DZ Levels of Theory

molecule	structure	state	PW91/LanL2DZ	PW91/aug-DZ
Cr_3F_6	T1	FM	0.029	0.041
	T1	AFM	0	0
	T2	FM	0.900	
	T2	AFM	0.885	
Cr_3Cl_6	T1	FM	0.030	0.105
	T1	AFM	0	0
	T2	FM	0.372	0.658
	T2	AFM	0.184	0.469
Cr_3Br_6	T1	FM	0.037	0.150
	T1	AFM	0	0.084
	T2	FM	0.241	0.463
	T2	AFM	0.004	0
Cr_3I_6	T1	FM	0.081	0.356
	T1	AFM	0.064	0.308
	T2	FM	0.087	0.419
	T2	AFM	0	0

The geometries of Cr_3F_6 and Cr_3Cl_6 (T1) are very similar to the dimers. There are three different Cr−Cr distances in the Cr_3Br_6 and Cr_3I_6 global minima (T2), with one being very short (2.462 Å for Cr_3Br_6 and 2.500 Å for Cr_3I_6), which is indicative of a metal−metal bond between the two Cr atoms, leading to larger spin-coupling and larger splitting between the AFM and the FM states. Indeed, the Cr_2-Cr_3 Wiberg bond indices with 0.42 (0.43) for $CrBr_2$ (CrI_2), respectively, support this finding.

The spins of (S_{Cr1}, S_{Cr2}, S_{Cr3}) in the AFM state of (T1) show a (2,-2,2) alignment, Supporting Information Table **S9**, and in (T2) we have (2,2,−2). The spin−spin interactions between Cr_1-Cr_2 and Cr_1-Cr_3 are different in (T2), and as a consequence we obtain quite different Cr_1-Cr_2 and Cr_1-Cr_3 bond lengths. We note that if we alter the spins to (2,−2,−2) for ($Cr_1Cr_2Cr_3$) in (T2), the resulting new quintet state is higher in energy. These results clearly demonstrate that there are greater exchange interactions between the Cr_2 and Cr_3 atoms in (T2) compared to those in the planar ribbons (T1).

Chromium Dihalide Tetramers. The coupling of four CrX_2 quintet units for the tetramers (Q) results in nine energetically low-lying spin states. The lowest energy AFM and FM structures for the tetramers Cr_4X_8 are shown in Figure 6. The relative energy ordering of the lowest energy tetramers is given in Table 6. A complete listing of the relative energies of all of the low-lying tetramers is located in the Supporting Information (Table **S10**). We obtain three major structures for the global and low-lying local minima. For Cr_4F_8 and Cr_4Cl_8, the lowest energy structure is, again, a continuation of the AFM planar structure (Q1). The global minimum for Cr_4Br_8 now consists of an intermediate spin-state (IM), (S_{Cr1}, S_{Cr2}, S_{Cr3}, S_{Cr4}) = (2,2,−2,2), of a nonplanar structure (Q4), and for Cr_4I_8, the AFM state of the non-planar (Q3) structure is the global minimum. However, for Cr_4Br_8 the corresponding AFM state of (Q4) is only 0.131 eV higher in energy than the IM state, and the FM state lies 0.454 eV above the global minimum. The IM and FM states for (Q3) of Cr_4I_8 are 0.024 and 0.516 eV higher in energy, respectively, compared to the global minimum. The latter value is rather large and may indicate that the correct FM ground state has not been correctly determined, as this becomes increasingly more difficult in a broken symmetry single determinant approach. The FM state of (Q3) shows inversion symmetry (C_i), while the AFM state breaks this symmetry. The primary structural difference between these tetramers is

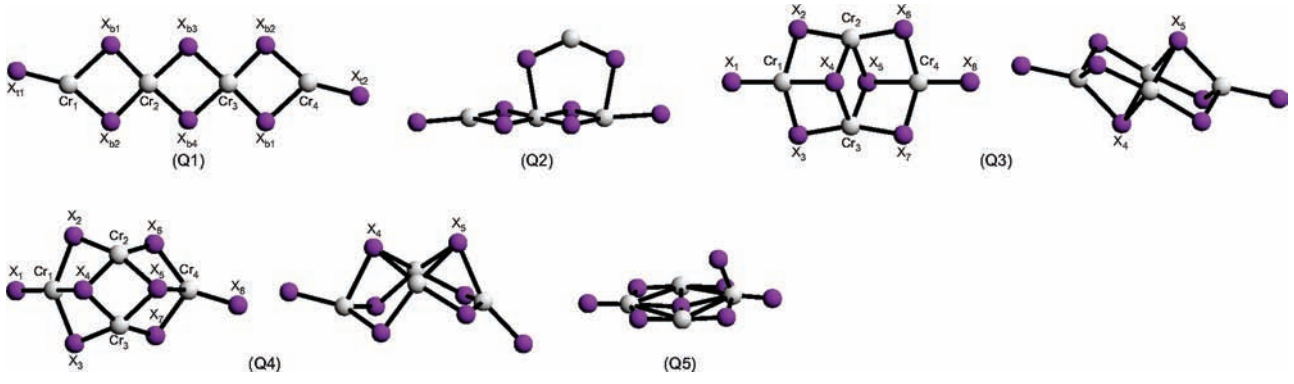

Figure 6. Low energy minima for the chromium dihalide tetramers.

Table 6. Relative Energies (eV) among the Lowest Energy Tetramers Shown in Figure 6 at the PW91/LanL2DZ and PW91/aug-DZ Levels of Theory

molecule	structure	state	PW91/ LanL2DZ	PW91/ aug-DZ
Cr_4F_8	Q1	FM	0.059	0.062
	Q1	IM	0.023	0.028
	Q1	AFM	0	0
	Q3	FM	0.429	0.904
	Q3	IM	0.331	0.882
	Q3	AFM	0.300	0.809
	Q4	FM	0.787	
	Q4	IM	0.424	
	Q4	AFM	0.618	
Cr_4Cl_8	Q1	FM	0.036	0.117
	Q1	IM	0.020	0.040
	Q1	AFM	0	0
	Q3	FM	0.398	
	Q3	AFM	0.327	
	Q4	FM	0.421	0.563
	Q4	IM	0.180	0.200
	Q4	AFM	0.284	0.196
Cr_4Br_8	Q1	FM	0.028	0.228
	Q1	IM	0.014	0.166
	Q1	AFM	0	0.124
	Q3	FM	0.361	
	Q3	IM	0.378	
	Q3	AFM	0.351	
	Q4	FM	0.270	0.454
	Q4	IM	0.207	0
	Q4	AFM	0.211	0.131
Cr_4I_8	Q1	FM	0.240	0.389
	Q1	IM	0.229	0.354
	Q1	AFM	0.213	0.332
	Q3	FM	0.304	0.516
	Q3	IM	0.256	0.024
	Q3	AFM	0.233	0
	Q4	FM	0.214	0.397
	Q4	IM	0	0.161
	Q4	AFM	0.098	0.286

that in (Q3), atoms X_4 and X_5 are *trans* to one another, and in (Q4), they are *cis*. Both (Q3) and (Q4) can be derived from the (T2) trimer by adding another CrX_2 unit to the cluster.

Selected geometrical parameters for the tetramer global minima are given in Supporting Information, Table **S11**. The Cr_4F_8 and Cr_4Cl_8 global minima (Q1) have two different Cr−Cr distances, with the Cr_1-Cr_2 and Cr_3-Cr_4 distances being different from the Cr_2-Cr_3 distance. However, the difference between the two Cr−Cr distances is rather small for Cr_4F_8, but becomes larger for Cr_4Cl_8, with a difference of about 0.15 Å. In comparison, with the continuation of the chain-like structure for these two systems, the Cr−X distances among the different oligomers change very little. Concerning the global minima of the $CrBr_2$ and CrI_2 tetramers, the Cr_1-Cr_2 and Cr_1-Cr_3, and the Cr_2-Cr_4 and Cr_3-Cr_4 distances are very close, respectively. Both of these tetramers contain a metal−metal bond between Cr_2 and Cr_3 with short bond distances of 2.592 Å for Cr_4Br_8 and 2.512 Å for Cr_4I_8. We note that atom Br_4 is bonded to Cr_1, Cr_2, and Cr_3 with bond lengths ranging between 2.56−2.63 Å. However, atom Br_5 is significantly further away from Cr_4 with a bond length of 2.83 Å. In Cr_4I_8, the three $Cr-I_4$ (and consequently the three $Cr-I_5$) distances are similar and between 2.72 and 2.78 Å. The terminal Cr_1-X_1 and Cr_4-X_8 bond lengths are the shortest of all of the Cr−X distances in Cr_4Br_8 and Cr_4I_8, and similar to the one calculated for the monomers.

The results of the Mulliken and NBO analyses for the tetramer global minima are given in Supporting Information, Table **S12**. For the CrF_2 tetramer, the pattern for (S_{Cr1}, S_{Cr2}, S_{Cr3}, S_{Cr4}) consists of (2,−2,2,−2), and for the $CrCl_2$ tetramer, we get preference for (2,−2,−2,2). The Cr_4Cl_8 spin-coupling pattern is similar to the antiferromagnetic intrachain spin-coupling scheme AFM-II we calculated previously for the solid state of α-$CrCl_2$.[29] However, this spin-coupling pattern did not give the lowest energy for the solid state, which is given by the AFM-I scheme (2,−2,2,−2,...). To determine if the spin-coupling pattern greatly influenced the energy of the weakly coupled structure (Q1), we altered the spin-coupling pattern for Cr_4F_8 to that of the AFM-II scheme while freezing its geometry to that of the ^1A_g state. This new coupling pattern was 0.028 eV above the AFM-I coupled state. After a geometry optimization, the AFM-II structure was only 0.017 eV above the global minimum, with the Cr_1-Cr_2 distance decreasing by 0.04 Å and the Cr_2-Cr_3 distance increasing by roughly 0.001 Å. A consequence of the AFM-II spin-coupling scheme is that the Cr_2-Cr_3 distance is longer than Cr_1-Cr_2 or Cr_3-Cr_4 (see Supporting Information, Table **S11**). The BS scheme for the IM state of Cr_4Br_8 (Q4) consists of a (2,2,−2,2) spin orientation scheme. The spin-coupling pattern for the AFM state of (Q4) is slightly different than that of the nonet. In this state, we have a (2,−2,−2,2) pattern for ($Cr_1Cr_2Cr_3Cr_4$). Both the nonet and singlet states of (Q4) have similar geometries, and we believe that the added instability of the AFM state is based on the much stronger spin−spin interactions between Cr_2 and Cr_3. To prove this, we look at the FM state of (Q4) for Cr_4Br_8, which is 0.454 eV higher in energy than the IM state. Hence, the spin−spin interactions between Cr_2 and Cr_3 are significant, which provides an explanation as to why the AFM state is higher in energy than the IM state for (Q4). At the PW91/LanL2DZ level, we were able to produce a (2,−2,2,−2) spin-coupling pattern for the AFM state of (Q4). This state was only 0.002 eV below the energy of the IM state for Cr_4Br_8 and 0.011 eV lower than the IM state for Cr_4I_8. Such small energy differences did not warrant a reinvestigation of the AFM state of (Q4) at the aug-DZ level of theory. Concerning the Cr_4I_8 AFM state (Q3) we have a (2,−2,2,−2) pattern, breaking C_i symmetry. Here the nonet state is only 0.024 eV higher in energy compared to the spin singlet. The spin-coupling scheme for the IM state is (2,−2,2,2). Like (Q4), the spin−spin interactions between Cr_2 and Cr_3 is significant, as the septendecet state for (Q3) is 0.516 eV higher in energy than the singlet state.

Thermodynamic Analysis. For a detailed thermodynamic analysis, a vibrational analysis is required and is briefly discussed here. The calculated vibrational frequencies for the monomers to the tetramers of the chromium dihalides can be found in the Supporting Information (Table **S13**). A more detailed discussion of the CrF_2 and $CrCl_2$ infrared spectra was also reported previously.[25,30] The vibrational data for the monomers show that the PW91 calculations overestimate the asymmetric stretching and underestimate the bending frequencies, and more accurate coupled-cluster calculations are required to obtain results in better agreement with experiment. Hence, we expect the same accuracy for the oligomers. The infrared spectra of the gas-phase chro-

mium dihalides are however complex, with several transitions arising from the different oligomers present in the vapor. A definite assignment of these transitions is therefore quite difficult. For example, our data for the $CrBr_2$ oligomers show that the IR spectrum consists of three intense peaks located at approximately 380, 340, and 310 cm^{-1}; the first peak comes from the asymmetric Cr−Br stretching mode of the monomer, and the remaining two come from the dimer and trimer. Kovba[20] studied the gas-phase IR spectrum of $CrBr_3$ and observed that it underwent decomposition to $CrBr_2$ and reacted with Br_2 gas to form $CrBr_4$. He concluded that the asymmetric stretching band from the $CrBr_2$ monomer was at 365 cm^{-1}. Kovba also observed bands at 320, 246, and 200 cm^{-1} and assigned these to the different vibrations from the dimer. We see that our monomer values are in good agreement; the dimer vibration at 320 cm^{-1} agrees reasonably well with our peak at 340 cm^{-1}. However, our data for the dimer does not show any absorptions around 246 or 200 cm^{-1}. Our calculated peak at 274 cm^{-1} is the only one that comes close to the experimental values for the dimer. However, for the trimer there are several absorptions around 246 and 200 cm^{-1}. Since this gas-phase IR experiment started with $CrBr_3$ and not from $CrBr_2$, the vapor composition may be complex, and we cannot ascertain whether the 246 and 200 cm^{-1} transitions come from the trimer or from other species present in the vapor.

The gas-phase IR absorption spectrum of CrI_2 vapor was obtained by Konings and Booij.[22] They observed the asymmetric stretching and bending peaks for the monomer at 319.7 and 37 cm^{-1}, respectively. We see that the asymmetric stretching frequency is in good agreement with our value, but the bending frequency is higher than our calculated value. They also observed three additional bands at 280.9 (intense), 214 cm^{-1} (weak), and 88 (weak) cm^{-1}. They concluded that the two bands at 280.9 and 88 cm^{-1} came from the dimeric species, and the one at 214 cm^{-1} came from the condensed phase. Looking at our calculated frequencies for the dimer, we see an intense band at 279 and a weak band at 96 cm^{-1}, which agree with the experimental data. However, a band at 242 cm^{-1} was not observed in their spectra, and this peak could have been buried underneath the strong absorption band at 280.9 cm^{-1}. We mention that Schiefenhövel and co-workers[31] calculated the IR spectra of the CrI_2 monomer and dimer with LDA. For the monomer, they calculated the frequencies to be at 70, 148, and 345 cm^{-1}, and for the dimer, they calculated the frequencies to be 19, 22, 38, 53, 72, 77, 108, 150, 215, 265, 305, and 336 cm^{-1}.

From the vibrational analyses and the calculated energy differences, we obtain ΔH, ΔG, ΔS, and dissociation energies (D_e) for the nucleation reactions (1) to (4) at 298.15 K which are listed in Table 7. The addition of each CrX_2 unit to the oligomers adds an almost constant value of 45−50 kcal/mol for all of the chromium dihalides. From a simple electrostatic model, we expect that the CrF_2 oligomers have the highest stability, with a steady decrease in dissociation energies going down the halide group. The D_e values for the CrF_2 oligomers are indeed approximately 5−10 kcal/mol higher than the rest of the chromium dihalides, with the exception of Cr_2F_4. Standard sublimation enthalpies of the chromium dihalides follow a similar pattern, that is, Brewer et al. tabulated the standard sublimation enthalpies of CrF_2, $CrCl_2$, $CrBr_2$, and CrI_2 to be 85, 64.8, 63.3, and 62 kcal/mol, respectively;[23,58] the CrF_2 value was an estimation only. These values are up to 20 kcal/mol higher than our results. Ratkovskii et al.[24] determined the standard enthalpies of dissociation for Cr_2Cl_4, Cr_3Cl_6, and Cr_4Cl_8 to be 55 ± 4, 109 ± 8, and 156 kcal/mol, respectively, from mass spectrometric studies. Using the ΔH values for the $CrCl_2$ oligomers listed in Table 7, we calculate dissociation enthalpies of 46.3, 90.8, and 135.7 kcal/mol, respectively. We find that our calculated enthalpies are about 10−20 kcal/mol too low. Hence, we followed a similar procedure as outlined in ref 25 by applying the CASPT2 D_e values for the dimers as a correction to the dissociation enthalpies. The CASPT2 D_e values along with the corrected dissociation energies (D_e') and reaction enthalpies ($\Delta H'$) for reactions 1 to 4 are also given in Table 7. We now obtain dissociation enthalpies of 52.7, 103.6, and 154.9 kcal/mol for Cr_2Cl_4, Cr_3Cl_6, and Cr_4Cl_8, respectively. These values are in much better agreement with those from the mass spectrometric studies. Schoonmaker

Table 7. Thermodynamic Values for the CrX_2 Nucleation from PW91 Calculations According to Reactions 1 to 4 in the Text at Standard Conditions (298.15 K and 1 atm)[a]

property	CrF_2	$CrCl_2$	$CrBr_2$	CrI_2
$D_e(1)$	44.6	46.7	45.6	43.3
$D_e'(1)$[b]	61.8	53.1	45.4	36.3
CASPT2 $D_e(1)$[c]	62.8	54.0	46.1	37.1
$\Delta H(1)$	−44.5	−46.3	−45.1	−42.9
$\Delta H'(1)$[b]	−61.7	−52.7	−44.9	−35.9
$\Delta G(1)$	−32.3	−35.1	−34.0	−33.4
$\Delta S(1)$	−40.8	−37.5	−37.2	−31.8
$D_e(2)$	49.1	44.8	43.5	45.8
$D_e'(2)$[b]	66.3	51.2	43.3	38.8
$\Delta H(2)$	−49.1	−44.5	−43.3	−45.4
$\Delta H'(2)$[b]	−66.3	−50.9	−43.1	−38.4
$\Delta G(2)$	−37.9	−34.1	−26.8	−29.0
$\Delta S(2)$	−37.7	−35.0	−55.1	−55.2
$D_e(3)$	49.2	45.3	44.6	40.6
$D_e'(3)$[b]	66.4	51.7	44.4	33.6
$\Delta H(3)$	−49.2	−44.9	−44.2	−40.2
$\Delta H'(3)$[b]	−66.4	−51.3	−44.0	−33.2
$\Delta G(3)$	−35.8	−32.4	−31.8	−26.8
$\Delta S(3)$	−44.8	−41.9	−41.1	−45.1
$D_e(4)$	53.7	43.4	42.5	43.1
$D_e'(4)$[b]	70.9	49.8	42.3	36.1
$\Delta H(4)$	−53.8	−43.1	−42.3	−42.7
$\Delta H'(4)$[b]	−71.0	−49.5	−42.1	−35.7
$\Delta G(4)$	−41.4	−31.4	−24.6	−22.3
$\Delta S(4)$	−35.8	−39.4	−59.3	−68.5

[a] D_e, ΔH, and ΔG in kcal/mol, ΔS in cal/mol K. The D_e values from PW91 calculations include the zero-point energy corrections. [b] CASPT2-corrected value. [c] The CASPT2 D_e values do not include zero-point energy corrections.

(58) (a) Brewer, L.; Somayajulu, G. R.; Brackett, E. *Chem. Rev.* **1963**, *63*, 111. (b) Allen, T. L. *J. Am. Chem. Soc.* **1956**, *78*, 5476. (c) Brewer, L.; Bromley, L. A.; Gilles, P. W.; Lofgren, N. L. *Chemistry and Metallurgy of Miscellaneous Materials*; McGraw-Hill: New York, 1995; Paper No. 6. (d) Doerner, A. H. *U.S. Bureau of Mines Technical Paper*, **1937**. (e) Gregory, N. W.; Burton, P. R. *J. Am. Chem. Soc.* **1953**, *75*, 6054. (f) Sime, R. J.; Gregory, N. W. *J. Am. Chem. Soc.* **1960**, *82*, 800.

et al.[23] determined that the ΔH_{298} for the dissociation of Cr_2Br_4 was 47.0 ± 3 kcal/mol from mass spectrometric studies. Our corrected $\Delta H'$ value of 43.1 kcal/mol is in good agreement with their value as well. Interestingly, if we look at the difference between the CASPT2 and PW91 D_e values for the dimers, we find that PW91 gives D_e values which are too small for Cr_2F_4 and Cr_2Cl_4. The D_e values for Cr_2Br_4 are roughly the same from both PW91 and CASPT2, and the PW91 value for Cr_2I_4 is slightly larger than the CASPT2 value.

From the Clusters to the Solid State. Our gas-phase calculations show that the AFM coupled ribbons of the chromium dihalides are either global minima or energetically very low-lying local minima. These ribbons are clearly seen in the chains formed in the corresponding crystal structures.[28,32] From our calculated data given in Table 2, we see that the PW91 functional overestimates the experimentally determined lattice parameters.[28,32] Correspondingly, the calculated equilibrium volumes for CrF_2, $CrCl_2$, $CrBr_2$, and CrI_2 are overestimated as well with 79.63 (77.74), 154.4 (138.2), 191.2 (161.1), and 239.4 (201.1) Å^3, respectively (experimental values set in parentheses). This overestimation coming from the PW91 functional was not apparent in the monomers where we obtained good agreement with the more accurate coupled cluster values. We obtain cohesive energies of 57.7, 45.9, 42.9, and 41.0 kcal/mol for CrF_2 to CrI_2, in the same range as the uncorrected nucleation energy obtained from reaction 3. We note, however, that the ribbons of CrF_2 units in the crystals are puckered in a zigzag pattern and are not fully planar like the rest of the dihalides. This structure allows for a more tightly packed crystal, which raises the sublimation energy. If we apply the CASPT2 correction to these cohesive energies, we obtain 74.9, 52.3, 42.7, and 34.0 kcal/mol for CrF_2, $CrCl_2$, $CrBr_2$, and CrI_2, respectively. These values are most likely still too low compared to the expected experimental sublimation energies.

According to our DFT calculations for the AFM coupled chain-like structures, the Cr−X bond distances for the bridging halides converge rapidly with increasing cluster size. However, these bonds are slightly shorter than the experimental values, as the solid-state interchain interactions are present. The deviations to the Cr−X_b bond lengths are however small and no more than 1.1%. Our solid-state calculations give intrachain Cr−X distances of 1.99, 2.36, 2.53, and 2.74 Å for CrF_2, $CrCl_2$, $CrBr_2$, and CrI_2, respectively in good agreement with the average Cr−X_b distances in the high-spin tetramers of 1.97, 2.38, 2.50, and 2.71 Å respectively.

Finally, we mention that the energy difference between the FM and AFM states for the tetramers (Q1) are 1.4 for CrF_2, 2.7 (0.8) for $CrCl_2$, 2.4 (0.4) for $CrBr_2$, and 1.3 (0.02) kcal/mol for CrI_2 (solid-state values are set in parentheses). Because of the unusual chain-like structure of CrF_2, we were unable to obtain an AFM coupling scheme for the solid state. For comparison, the experimental energy difference between the AFM and FM spin-coupling patterns at 298 K for $CrCl_2$ is 0.009 eV.[27] It is well-known that BS-DFT overestimates such energy differences.[55]

Conclusions

The study of nucleation of transition metal halides remains a challenging task both experimentally and theoretically, as shown for the chromium halides in this work. Even the monomers are difficult to describe correctly by quantum theoretical methods because of shallow bending potentials and many low-lying excited electronic states. Hence, accurate multireference procedures are required to fully understand the properties of these molecules. Our DFT and CCSD(T) calculations both show that the global minimum of the monomer is of $^5B_2$ symmetry arising from the Renner−Teller distorted $^5\Pi_g$ saddle point with very shallow bending potentials. At high temperatures, they would be best described as having quasi-linear structures. Because high temperatures are required to vaporize these substances, the concept of a single-state approach to interpret the experiments breaks down, and one needs to consider all low lying minima of different spin states. Future measurements of low-temperature vibrational−rotational spectra should help to interpret the different electronic states and corresponding structures.

The global minima of the CrF_2 and $CrCl_2$ clusters consist of planar ribbons of (most likely) AFM coupled CrX_2 units, with their structures having a striking similarity to their crystals. These planar ribbons were also low-lying minima for the clusters of $CrBr_2$ and CrI_2; however, the "triangular" geometry (structures (T3), (Q3), (Q4)) takes precedence over the planar ribbons for their trimers and tetramers. We find that each CrX_2 unit adds an almost constant energy to the clusters, with each CrX_2 unit adding between 45 and 50 kcal/mol. Even more interesting is that the sublimation energies of the chromium dihalides follows a similar pattern, with CrF_2 having the highest and $CrCl_2$ to CrI_2 having similar sublimation energies. Looking at their crystal structures, the large difference in sublimation energy for CrF_2 is likely due to the high electronegativity of fluorine along with a more tightly packed crystal structure. The structural similarities among the low-lying chain-like solid-state structures are already apparent early in the nucleation processes of the chromium dihalide clusters. The calculated cohesive energies show that they decrease going down the halide group, as one expects from simple electrostatic interactions. We realize that the broken-symmetry DFT approach is not ideal for the correct description of the spin-coupling between the different CrX_2 units, but we only managed CASPT2 calculations with a small restricted CAS for the dimer. For predicting the correct spin state and structure for each of these clusters, much more computational work needs to be done. Any other calculations for the larger clusters would have been prohibitive in computer time. We conclude that correctly describing spin-coupling in the solid-state through wave function based methods remains a challenge for future investigations. Of course, nucleation is a dynamic process, and it would be highly desirable to perform molecular dynamic simulation of cluster growth for transition metal containing compounds, which is currently beyond our computational means.

Acknowledgment. We thank Prof. M. Hargittai (Budapest) for useful discussions and for originally initiating this project, and one referee for an interesting ongoing and lengthy debate. Financial support from the Marsden Fund (Wellington) is gratefully acknowledged.

Supporting Information Available: Listings of the BSSE analysis, energetic, geometric, and vibrational data from various DFT and wave function-based calculations for $CrBr_2$ and CrI_2, the relative energies among all of the low-lying chromium dihalide oligomers from PW91 calculations, and PW91 vibrational frequencies for all global minima. This material is available free of charge via the Internet at http://pubs.acs.org.